

Causal dissipative hydrodynamics for QGP fluid in 2+1 dimensions

A. K. Chaudhuri*

Variable Energy Cyclotron Centre, 1/AF, Bidhan Nagar, Kolkata 700 064, India

(Dated: February 21, 2013)

In 2nd order causal dissipative theory, space-time evolution of QGP fluid is studied in 2+1 dimensions. Relaxation equations for shear stress tensors are solved simultaneously with the energy-momentum conservation equations. Comparison of evolution of ideal and viscous QGP fluid, initialized under the same conditions, e.g. same equilibration time, energy density and velocity profile, indicate that in a viscous dynamics, energy density or temperature of the fluid evolve slowly, than in an ideal fluid. Cooling gets slower as viscosity increases. Transverse expansion also increases in a viscous dynamics. For the first time we have also studied elliptic flow of 'quarks' in causal viscous dynamics. It is shown that elliptic flow of quarks saturates due to non-equilibrium correction to equilibrium distribution function, and can not be mimicked by an ideal hydrodynamics.

PACS numbers: 47.75.+f, 25.75.-q, 25.75.Ld

I. INTRODUCTION

One of the most important discoveries in Relativistic Heavy ion collider (RHIC) at Brookhaven National Laboratory is the large elliptic flow in non-central Au+Au collisions [1, 2, 3, 4]. Elliptic flow measures the momentum anisotropy of produced particles and is quantified by the 2nd harmonic of the azimuthal distribution,

$$v_2(p_T) = \langle \cos(2\phi) \rangle = \frac{\int_0^{2\pi} \frac{dN}{dyd^2p_T} \cos(2\phi) d\phi}{\int_0^{2\pi} \frac{dN}{dyd^2p_T} d\phi} \quad (1.1)$$

Elliptic flow is naturally explained in hydrodynamics. Hydrodynamic pressure is built up from rescattering of secondaries, and pressure gradients drive the subsequent collective motion. In non-central Au+Au collisions, initially, the reaction zone is asymmetric (almond shaped). The pressure gradient is large in one direction and small in the other. The asymmetric pressure gradients generates the elliptic flow. Naturally, in a central collision, reaction zone is symmetric and elliptic flow vanishes. Observed elliptic flow then give the strongest indication that in non-central Au+Au collisions, a collective QCD matter is produced. Whether the formed matter can be identified as the much sought after Quark-Gluon Plasma (QGP) as predicted in Lattice QCD simulations [5] is presently debatable.

Ideal hydrodynamics has been partly successful in explaining the observed elliptic flow, quantitatively [6]. Elliptic flow of identified particles, up to $p_T \sim 1.5$ GeV are well reproduced in ideal hydrodynamics. Ideal hydrodynamics also explains the transverse momentum spectra of identified particles (up to $p_T \sim 1.5$ GeV). Success of *ideal* hydrodynamics in explaining bulk of the data [6], together with the string theory motivated lower limit of

shear viscosity $\eta/s \geq 1/4\pi$ [7, 8] has led to a paradigm that in Au+Au collisions, a nearly perfect fluid is created.

However, the paradigm of "perfect fluid" produced in Au+Au collisions at RHIC need to be clarified. As indicated above, the ideal hydrodynamics is only partially successful and in a limited p_T range ($p_T \leq 1.5$ GeV) [9]. The transverse momentum spectra of identified particles also starts to deviate from ideal fluid dynamics prediction beyond $p_T \approx 1.5$ GeV. Experimentally determined HBT radii are not reproduced in the ideal fluid dynamic models, the famous "HBT puzzle" [10]. It also do not reproduce the experimental trend that elliptic flow saturates at large transverse momentum. These shortcomings of ideal fluid dynamics indicate greater importance of dissipative effects in the p_T ranges greater than 1.5 GeV or in more peripheral collisions. Indeed, ideal fluid is a concept, never realized in nature. As suggested in string theory motivated models [7, 8], QGP viscosity could be small, $\eta/s \geq 1/4\pi$, nevertheless it is non-zero. It is important to study the effect of viscosity, even if small, on space-time evolution of QGP fluid and quantify its effect. This requires a numerical implementation of relativistic dissipative fluid dynamics. Furthermore, if QGP fluid is formed in heavy ion collisions, it has to be characterized by measuring its transport coefficients, e.g. heat conductivity, bulk and shear viscosity. Theoretically, it is possible to obtain those transport coefficients in a kinetic theory model. However, in the present status of theory, the goal can not be achieved immediately, even more so for a strongly interacting QGP (sQGP). Alternatively, one can use the experimental data to obtain a "phenomenological" limit of transport coefficients of sQGP. It will also require a numerical implementation of relativistic dissipative fluid dynamics. There is another incentive to study dissipative hydrodynamics. Ideal hydrodynamics depends on the assumption of local equilibrium. Before local equilibrium is attained, the system has to pass through a non-equilibrium stage, where (if non-equilibrium effects are small) dissipative hydrodynamics may be applicable. Indeed, we can explore early times of fluid evolution better in a dissipative hydrodynamics.

*E-mail: akc@veccal.ernet.in

Theory of dissipative relativistic fluid has been formulated quite early. The original dissipative relativistic fluid equations were given by Eckart [11] and Landau and Lifshitz [12]. They are called 1st order theories. Formally, relativistic dissipative hydrodynamics are obtained from an expansion of entropy 4-current, in terms of dissipative fluxes. In 1st order theories, entropy 4-current contains terms linear in dissipative quantities. 1st order theory of dissipative hydrodynamics suffer from the problem of causality violation. Signal can travel faster than light. Causality violation is unwarranted in any theory, even more in a relativistic theory. The problem of causality violation is removed in the Israel-Stewart's 2nd order theory of dissipative fluid [13]. In 2nd order theory, expansion of entropy 4-current contains terms 2nd order in dissipative fluxes. However, these leads to complications that dissipative fluxes are no longer function of the state variables only. They become dynamic. The space of thermodynamic variables has to be extended to include the dissipative fluxes (e.g. heat conductivity, bulk and shear viscosity).

Even though 2nd order theory was formulated some 30 years back, significant progress towards its numerical implementation has only been made very recently [14, 15, 16, 17, 18, 19, 20, 21, 22, 23]. At the Cyclotron Centre, Kolkata, we have developed a code "AZHYDRO-KOLKATA" to simulate the hydrodynamic evolution of dissipative QGP fluid. Presently only dissipative effect included is the shear viscosity. Some results of AZHYDRO-KOLKATA, for first order dissipative hydrodynamics have been published earlier [19, 20, 21]. In the present paper, for the first time, we will present some results for 2nd order dissipative hydrodynamics in 2+1 dimensions. In the present paper, we will consider effect of dissipation in the QGP phase only. Effect of phase transition will be studied in a later publication.

The paper is organized as follows: In section II we briefly review relativistic dissipative fluid dynamics. In section III we derive the relevant equations in 2+1 dimension (assuming boost-invariance). Required inputs e.g. the equation of state, viscosity coefficient and initial conditions are discussed in section IV. Simulation results from AZHYDRO-KOLKATA are shown in section V. In section VII we compare the transverse momentum spectra and elliptic flow of quarks in ideal and viscous dynamics. The concluding section IX summarizes our results.

II. DISSIPATIVE FLUID DYNAMICS

In this section, I briefly discuss the phenomenological theory of dissipative hydrodynamics. More detailed exposition can be found in [13].

A simple fluid, in an arbitrary state, is fully specified by primary variables: particle current (N^μ), energy-momentum tensor ($T^{\mu\nu}$) and entropy current (S^μ) and a number of additional (unknown) variables. Primary

variables satisfies the conservation laws;

$$\partial_\mu N^\mu = 0, \quad (2.1)$$

$$\partial_\mu T^{\mu\nu} = 0, \quad (2.2)$$

and the 2nd law of thermodynamics,

$$\partial_\mu S^\mu \geq 0. \quad (2.3)$$

In relativistic fluid dynamics, one defines a time-like hydrodynamic 4-velocity, u^μ (normalized as $u^2 = 1$). One also define a projector, $\Delta^{\mu\nu} = g^{\mu\nu} - u^\mu u^\nu$, orthogonal to the 4-velocity ($\Delta^{\mu\nu} u_\nu = 0$). In equilibrium, an unique 4-velocity (u^μ) exists such that the particle density (n), energy density (ε) and the entropy density (s) can be obtained from,

$$N_{eq}^\mu = n u_\mu \quad (2.4)$$

$$T_{eq}^{\mu\nu} = \varepsilon u^\mu u^\nu - p \Delta^{\mu\nu} \quad (2.5)$$

$$S_{eq}^\mu = s u_\mu \quad (2.6)$$

An equilibrium state is assumed to be fully specified by 5-parameters, (n, ε, u^μ) or equivalently by the thermal potential, $\alpha = \mu/T$ (μ being the chemical potential) and inverse 4-temperature, $\beta^\mu = u^\mu/T$. Given a equation of state, $s = s(\varepsilon, n)$, pressure p can be obtained from the generalized thermodynamic relation,

$$S_{eq}^\mu = p \beta^\mu - \alpha N_{eq}^\mu + \beta_\lambda T_{eq}^{\lambda\mu} \quad (2.7)$$

Using the Gibbs-Duhem relation, $d(p\beta^\mu) = N_{eq}^\mu d\alpha - T_{eq}^{\lambda\mu} d\beta_\lambda$, following relations can be established on the equilibrium hyper-surface $\Sigma_{eq}(\alpha, \beta^\mu)$,

$$dS_{eq}^\mu = -\alpha dN_{eq}^\mu + \beta_\lambda dT_{eq}^{\lambda\mu} \quad (2.8)$$

In a non-equilibrium system, no 4-velocity can be found such that Eqs.2.4,2.5,2.6 remain valid. Tensor decomposition leads to additional terms,

$$N^\mu = N_{eq}^\mu + \delta N^\mu = n u^\mu + V^\mu \quad (2.9)$$

$$\begin{aligned} T^{\mu\nu} &= T_{eq}^{\mu\nu} + \delta T^{\mu\nu} \\ &= [\varepsilon u^\mu u^\nu - p \Delta^{\mu\nu}] + \Pi \Delta^{\mu\nu} + \pi^{\mu\nu} \\ &\quad + (W^\mu u^\nu + W^\nu u^\mu) \end{aligned} \quad (2.10)$$

$$S^\mu = S_{eq}^\mu + \delta S^\mu = s u^\mu + \Phi^\mu \quad (2.11)$$

The new terms describe a net flow of charge $V^\mu = \Delta^{\mu\nu} N_\nu$, heat flow, $W^\mu = (\varepsilon + p)/n V^\mu + q^\mu$ (where q^μ is the heat flow vector), and entropy flow Φ^μ . $\Pi = -\frac{1}{3} \Delta_{\mu\nu} T^{\mu\nu} - p$ is the bulk viscous pressure and $\pi^{\mu\nu} = [\frac{1}{2} (\Delta^{\mu\sigma} \Delta^{\nu\tau} + \Delta^{\nu\sigma} \Delta^{\mu\tau} - \frac{1}{3} \Delta^{\mu\nu} \Delta^{\sigma\tau}) T_{\sigma\tau}$ is the shear stress tensor. Hydrodynamic 4-velocity can be chosen to eliminate either V^μ (the Eckart frame, u^μ is parallel to particle

flow) or the heat flow q^μ (the Landau frame, u^μ is parallel to energy flow). In relativistic heavy ion collisions, central rapidity region is nearly baryon free and Landau's frame is more appropriate than the Eckart's frame. Dissipative flows are transverse to u^μ and additionally, shear stress tensor is traceless. Thus a non-equilibrium state require $1+3+5=9$ additional quantities, the dissipative flows Π , q^μ (or V^μ) and $\pi^{\mu\nu}$. In kinetic theory, N^μ and $T^{\mu\nu}$ are the 1st and 2nd moment of the distribution function. Unless the function is known a-priori, two moments do not furnish enough information to enumerate the microscopic states required to determine S^μ , and in an arbitrary non-equilibrium state, no relation exists between, N^ν , $T^{\mu\nu}$ and S^μ . *Only in a state, close to a equilibrium one, such a relation can be established.* Assuming that the equilibrium relation Eq.2.8 remains valid in a "near equilibrium state" also, the entropy current can be generalized as,

$$S^\mu = S_{eq}^\mu + dS^\mu = p\beta^\mu - \alpha N^\mu + \beta_\lambda T^{\lambda\mu} + Q^\mu \quad (2.12)$$

where Q^μ is an undetermined quantity in 2nd order in deviations, $\delta N^\mu = N^\mu - N_{eq}^\mu$ and $\delta T^{\mu\nu} = T^{\mu\nu} - T_{eq}^{\mu\nu}$. Detail form of Q^μ is constrained by the 2nd law $\partial_\mu S^\mu \geq 0$. With the help of conservation laws and Gibbs-Duhem relation, entropy production rate can be written as,

$$\partial_\mu S^\mu = -\delta N^\mu \partial_\mu \alpha + \delta T^{\mu\nu} \partial_\mu \beta_\nu + \partial_\mu Q^\mu \quad (2.13)$$

Choice of Q^μ leads to 1st order or 2nd order theories of dissipative hydrodynamics. In 1st order theories the simplest choice is made, $Q^\mu = 0$, entropy current contains terms up to 1st order in deviations, δN^μ and $\delta T^{\mu\nu}$. Entropy production rate can be written as,

$$T\partial_\mu S^\mu = \Pi X - q^\mu X_\mu + \pi^{\mu\nu} X_{\mu\nu} \quad (2.14)$$

where, $X = -\nabla \cdot u$; $X^\mu = \frac{\nabla^\mu}{T} - u^\nu \partial_\nu u^\mu$ and $X^{\mu\nu} = \nabla^{<\mu} u^{\nu>}$.

The 2nd law, $\partial_\mu S^\mu \geq 0$ can be satisfied by postulating a linear relation between the dissipative flows and thermodynamic forces,

$$\Pi = -\zeta\theta, \quad (2.15)$$

$$q^\mu = -\lambda \frac{nT^2}{\varepsilon + p} \nabla^\mu (\mu/T), \quad (2.16)$$

$$\pi^{\mu\nu} = 2\eta \nabla^{<\mu} u^{\nu>} \quad (2.17)$$

where ζ , λ and η are the positive transport coefficients, bulk viscosity, heat conductivity and shear viscosity respectively.

In 1st order theories, causality is violated. If, in a given fluid cell, at a certain time, thermodynamic forces vanish, corresponding dissipative fluxes also vanish instantly. Violation of causality is unwanted in any theory, even more

so in relativistic theory. Causality violation of dissipative hydrodynamics is corrected in 2nd order theories [13]. In 2nd order theories, entropy current contain terms up to 2nd order in the deviations, $Q^\mu \neq 0$. The most general Q^μ containing terms up to 2nd order in deviations can be written as,

$$Q^\mu = -(\beta_0 \Pi^2 - \beta_1 q^\nu q_\nu + \beta_2 \pi_{\nu\lambda} \pi^{\nu\lambda}) \frac{u^\mu}{2T} - \frac{\alpha_0 \Pi q^\mu}{T} + \frac{\alpha_1 \pi^{\mu\nu} q_\nu}{T} \quad (2.18)$$

As before, one can cast the entropy production rate ($T\partial_\mu S^\mu$) in the form of Eq.2.14. Neglecting the terms involving dissipative flows with gradients of equilibrium thermodynamic quantities (both are assumed to be small) and demanding that a linear relation exists between the dissipative flows and thermodynamic forces, following *relaxation* equations for the dissipative flows can be obtained,

$$\Pi = -\zeta(\theta + \beta_0 D\Pi) \quad (2.19)$$

$$q^\mu = -\lambda \left[\frac{nT^2}{\varepsilon + p} \nabla^\mu (\frac{\mu}{T}) - \beta_1 Dq^\mu \right] \quad (2.20)$$

$$\pi^{\mu\nu} = 2\eta [\nabla^{<\mu} u^{\nu>} - \beta_2 D\pi_{\mu\nu}], \quad (2.21)$$

where $D = u^\mu \partial_\mu$ is the convective time derivative. Unlike in the 1st order theories, in 2nd order theories, dynamical equations control the dissipative flows. Even if thermodynamic forces vanish, dissipative flows do not vanish instantly.

Before we proceed further, it may be mentioned that the parameters, α and β_λ are not connected to the actual state ($N^\mu, T^{\mu\nu}$). The pressure p in Eq.2.12 is also not the "actual" thermodynamics pressure, i.e. not the work done in an isentropic expansion. Chemical potential α and 4-inverse temperature β_λ has meaning only for the equilibrium state. Their meaning need not be extended to non-equilibrium states also. However, it is possible to fit a fictitious "local equilibrium" state, point by point, such that pressure p in Eq.2.12 can be identified with the thermodynamic pressure, at least up to 1st order. The conditions of fit fixes the underlying non-equilibrium phase-space distribution.

III. (2+1)-DIMENSIONAL VISCOUS HYDRODYNAMICS WITH LONGITUDINAL BOOST INVARIANCE

Complete dissipative hydrodynamics is a numerically challenging problem. It requires simultaneous solution of 14 partial differential equations (5 conservation equations and 9 relaxation equations for dissipative flows). We reduce the problem to solution of 6 partial differential equations (3 conservation equations and 3 relaxation equations). In the following, we will study boost-invariant evolution of baryon free QGP fluid, including the dissipative effect due to shear viscosity only. Shear viscosity

is the most important dissipative effect. For example, in a baryon free QGP, heat conduction is zero and we can disregard Eq.2.20. Bulk viscosity is also zero for the QGP fluid (point particles) and Eq.2.19 can also be neglected. Shear pressure tensor has 5 independent components but the assumption of boost invariance reduces the number of independent components to three. For a baryon free fluid, we can also disregard the conservation equation Eq.2.1. With the assumption of boost-invariance, energy-momentum conservation equation $\partial_\mu T^{\mu\eta} = 0$ become redundant and only three energy-momentum conservation equations are required to be solved.

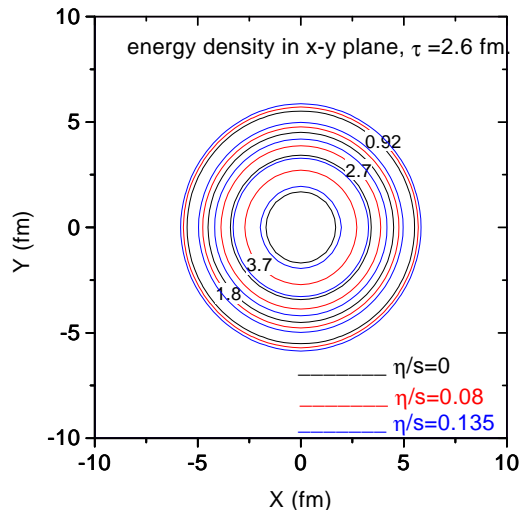


FIG. 1: (color online). Constant energy density contours in x-y plane at $\tau=2.6$ fm. The black lines are for ideal fluid ($\eta/s=0$). The red and blue lines are for viscous fluid with ADS/CFT and perturbative estimate of viscosity, $\eta/s=0.08$ and 0.135.

Heavy ion collisions are best described in (τ, x, y, η) coordinates, where $\tau = \sqrt{t^2 - z^2}$ is the longitudinal proper time and $\eta = \frac{1}{2} \ln \frac{t+z}{t-z}$ is the space-time rapidity. $r_\perp = (x, y)$ are the usual cartesian coordinate in the plane, transverse to the beam direction. Relevant equations concerning this coordinate transformations are given in the appendix A.

Explicit equations for energy-momentum conservation in (τ, x, y, η) coordinates are given in the appendix B. We note that unlike in ideal fluid, in viscous fluid dynamics, conservation equations (see Eqs.B1-B3) contain additional pressure gradients due to shear viscosity. Both $T^{\tau x}$ and $T^{\tau y}$ components of energy-momentum tensor now evolve under additional pressure gradients. The right-most term of Eq.B3 also indicate that in viscous dynamics, longitudinal pressure is effectively reduced (note that the $\pi^{\eta\eta}$ component is negative). Since pressure can not be negative, shear viscosity is limited by the condition, $p + \tau^2 \pi^{\eta\eta} \geq 0$.

As evident from the Eqs.B1-B3, in boost-invariant dissipative hydrodynamics, with shear viscosity taken into

account, fluid evolution depends only on seven components of the shear stress tensors. They are $\pi^{\tau\tau}$, $\pi^{\tau x}$, $\pi^{\tau y}$, π^{xx} , π^{yy} , π^{xy} and $\pi^{\eta\eta}$. However, all the seven components are not independent. Tracelessness, transversality to u^μ and the assumption of boost-invariance reduces the independent components to three. Presently, we choose π^{xx} , π^{yy} and π^{xy} as the independent components. Relaxation equations for the independent components are given in the appendix C (see Eqs.C4-C6). They are solved simultaneously with the three energy momentum conservation equations Eqs.B1-B3, with inputs as discussed below.

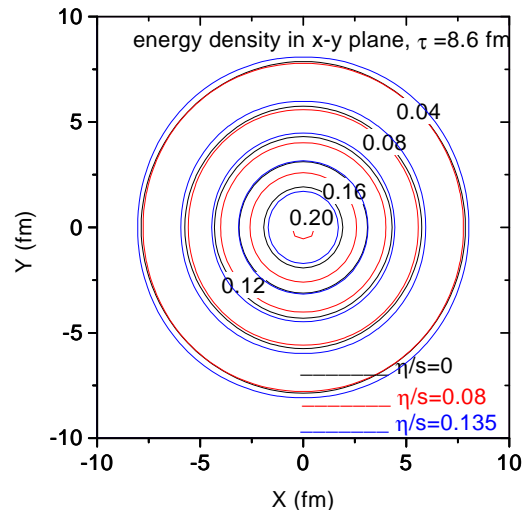


FIG. 2: (color online). same as Fig.1 but at time $\tau=8.6$ fm.

IV. EQUATION OF STATE, VISCOSITY COEFFICIENT AND INITIAL CONDITIONS

A. Equation of state

One of the most important inputs of a hydrodynamic model is the equation of state. Through this input, the macroscopic hydrodynamic models make contact with the microscopic world. In the present demonstrative calculation we will show results for the QGP phase only. In the QGP phase, we use the simple equation of state, $p = \frac{1}{3}\epsilon$, with energy density given as,

$$\epsilon = \frac{\pi^2}{30} g_{qgp} T^4 \quad (4.1)$$

where $g_{qgp} = g_{gluon} + \frac{7}{8} g_{quark}$ is the degeneracy factor for QGP. $g_{gluon} = 2(\text{helicity}) \times 8(\text{color})$ is the degeneracy factor for gluons and $g_{quark} = 2(\text{spin}) \times 3(\text{color}) \times 2(q + \bar{q}) \times N_f$ is the degeneracy factor for N_f flavored quarks. For $N_f \approx 2.5$, the degeneracy factor is $g_{qgp} = 42.25$

B. Shear viscosity coefficient

Shear viscosity coefficient (η) of QGP or sQGP is quite uncertain. In a strongly coupled QGP, shear viscosity can not be computed. Recently, using the ADS/CFT correspondence [7, 8] shear viscosity of a strongly coupled gauge theory, N=4 SUSY YM, has been evaluated, $\eta = \frac{\pi}{8} N_c^2 T^3$ and the entropy is given by $s = \frac{\pi^2}{2} N_c^2 T^3$. Thus in the strongly coupled field theory,

$$\left(\frac{\eta}{s}\right)_{ADS/CFT} = \frac{1}{4\pi} \approx 0.08, \quad (4.2)$$

Shear viscosity is quite uncertain in perturbative QCD also. At high temperature, shear viscosity, in leading log, can be written as [24, 25],

$$\eta = \kappa \frac{T^3}{g^4 \ln g^{-1}}, \quad (4.3)$$

where g is the strong coupling constant. The leading log shear viscosity coefficient κ depend on the number of fermion flavors (N_f). For example, for two flavored QGP, $\kappa = 86.47$ and $\kappa = 106.7$ for a three flavored QGP. With entropy density of QGP, $s = \frac{\pi^2}{15} g_{qgp} T^3$. For two flavored QGP and $\alpha_s \approx 0.5$, the ratio of viscosity over the entropy, in the perturbative regime is estimated as,

$$\left(\frac{\eta}{s}\right)_{pert} \approx 0.135, \quad (4.4)$$

For lower α_s , perturbative estimation of η/s could be even higher.

Shear viscosity can also be expressed in terms of sound attenuation length, Γ_s , defined as,

$$\Gamma_s = \frac{4\eta}{3sT} \quad (4.5)$$

Γ_s is equivalent to mean free path and for a valid hydrodynamic description $\Gamma_s/\tau \ll 1$, i.e. mean free path is much less than the system size. Initial conditions of the fluid must be chosen carefully such that the validity condition $\Gamma_s/\tau \ll 1$ remains valid initially as well as at later time also. In the present work, we have treated viscosity as a parameter. To explore the effect of viscosity, we have used both the ADS/CFT estimate $\eta/s=0.08$ and perturbative estimate $\eta/s=0.135$. We have also run the code with a higher value of viscosity $\eta/s=0.2$.

C. Initial conditions

Solution of Eqs.B1-B3 require initial conditions, the initial time τ_i , the transverse distribution of energy density $\varepsilon(x, y)$ and the velocities $v_x(x, y)$ and $v_y(x, y)$. Following [6], initial transverse energy density is parameterized geometrically. At an impact parameter \vec{b} , transverse distribution of wounded nucleons $N_{WN}(x, y, \vec{b})$ and

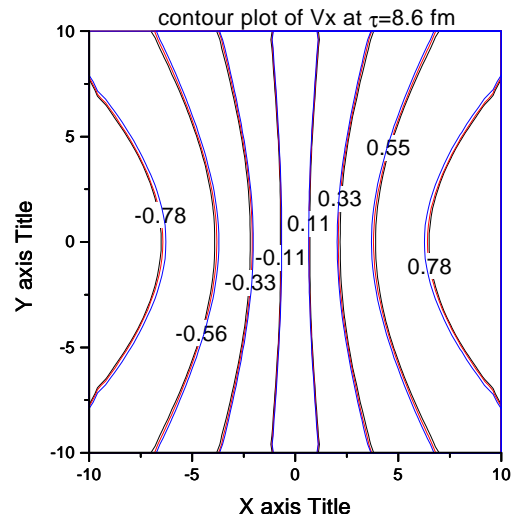


FIG. 3: (color online). contours of constant v_x in x-y plane at $\tau=8.6$ fm. The black lines are for ideal fluid ($\eta/s=0$). The red and blue lines are for viscous fluid with ADS/CFT and perturbative estimate of viscosity, $\eta/s=0.08$ and 0.135 .

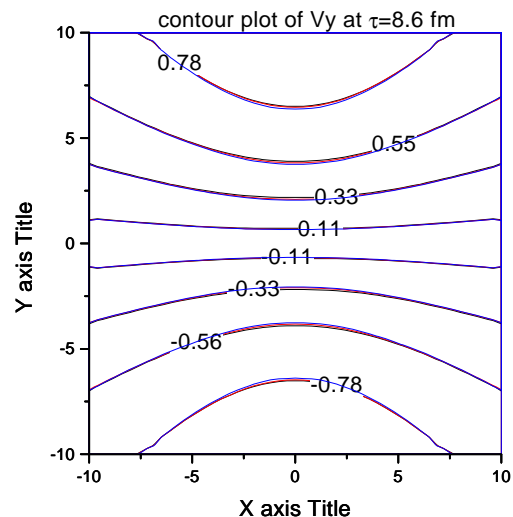


FIG. 4: (color online). contours of constant v_y in x-y plane at $\tau=8.6$ fm. The black lines are for ideal fluid ($\eta/s=0$). The red and blue lines are for viscous fluid with ADS/CFT and perturbative estimate of viscosity, $\eta/s=0.08$ and 0.135 .

of binary NN collisions $N_{BC}(x, y, \vec{b})$ to are calculated in a Glauber model. A collision at impact parameter \vec{b} is assumed to contain 25% hard scattering (proportional to number of binary collisions) and 75% soft scattering (proportional to number of wounded nucleons). Transverse energy density profile at impact parameter \vec{b} is then obtained as,

V. RESULTS

VI. STABILITY OF NUMERICAL SOLUTIONS

A. Evolution of the viscous QGP fluid

The energy-momentum conservation equations B1-B3, and the relaxation equations C2-C4 are solved simultaneously using the code, AZHYDRO-KOLKATA, developed at the Cyclotron Centre, Kolkata. As mentioned earlier, we have solved the equations in the QGP phase only and did not consider any phase transition. In the following we will show the results for central Au+Au collisions (impact parameter $b = 0$ fm). To understand the effect of shear viscosity, with the same initial conditions, we have solved the energy-momentum conservation equations for ideal fluid and viscous fluid. As mentioned earlier, we have considered two values of viscosity, the ADS/CFT motivated value $\eta/s=0.08$ and the perturbative estimate, $\eta/s=0.135$.

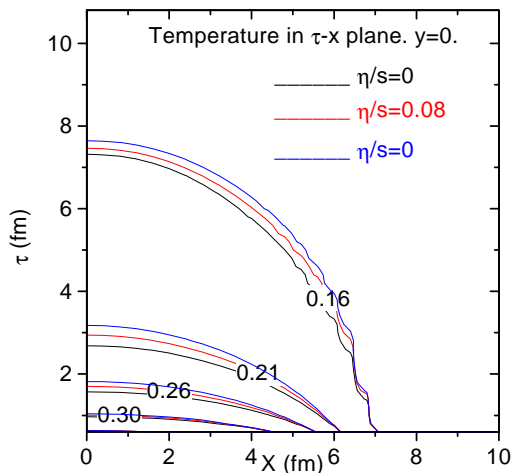


FIG. 5: (color online). Constant temperature contour in $x - \tau$ plane, for fixed $y=0$. The black, red and blue lines are for ideal, viscous fluid with $\eta/s=0.08$ and viscous fluid with $\eta/s=0.135$.

In dissipative hydrodynamics, one requires initial conditions for the viscous pressures also. Due to longitudinal boost invariance of the problem, we assume that viscous pressures have attained their boost-invariant values at the time of equilibration. Boost invariant values of the three independent shear stress-tensors can be easily obtained from Eqs.C4-C6, $\sigma^{xx} = \sigma^{yy} = \theta = \frac{1}{\tau_i}$ and $\sigma^{xy} = 0$ (at the initial time τ_i , $u^\mu = (1, 0, 0, 0)$, $\bar{D}u^\mu = 0$). The initial distribution of shear pressure tensors are then obtained as,

$$\pi^{xx}(x, y, \vec{b}) = 2\eta\sigma^{xx} = 2\eta/\tau_i \quad (4.7)$$

$$\pi^{yy}(x, y, \vec{b}) = 2\eta\sigma^{yy} = 2\eta/\tau_i \quad (4.8)$$

$$\pi^{xy}(x, y, \vec{b}) = 2\eta\sigma^{xy} = 0 \quad (4.9)$$

As stated earlier, the viscous coefficient η is obtained using the relation, $\eta/s = \text{const}$, $\text{const}=0.08, 0.135$ or 0.2 . For these values of shear viscosity, the validity condition $\Gamma_s/\tau \ll 1$ is satisfied initially. The validity condition is better satisfied at later time.

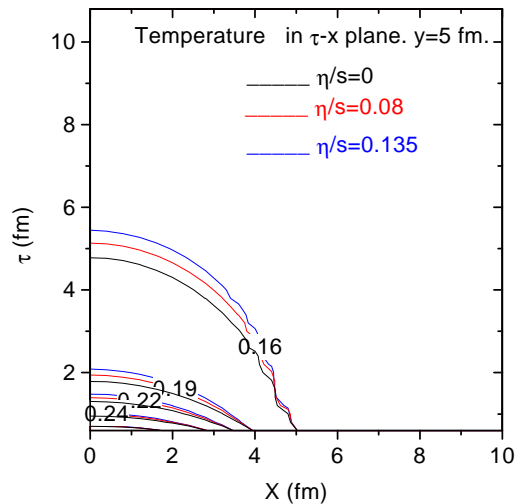


FIG. 6: (color online). same as fig.5 but at $y=5.0$

In Fig.1, we have shown the contours of constant energy density in x-y plane, after an evolution of 2.6 fm. The black lines are for ideal fluid evolution. The red and blue lines are for viscous fluid with ADS/CFT ($\eta/s=0.08$) and perturbative ($\eta/s=0.135$) estimate of viscosity. Constant energy density contours, as depicted in Fig.1, indicate that with viscosity fluid cools slowly. Cooling gets slower as viscosity increases. Thus at any point in the x-y plane, energy density of viscous fluid is higher than that of an ideal fluid. At later time also, compared to an ideal fluid, viscous fluid evolve slowly. In Fig.2, contours of constant energy density at time $\tau=8.6$ fm is shown. Here also we find that at any point energy density of viscous fluid is higher than its ideal counter part. The result is in accordance with our expectation. For dissipative fluid, equation of motion can be written as,

$$D\varepsilon = -(\varepsilon + p)\nabla_\mu u^\mu + \pi^{\mu\nu}\nabla_{<\mu}u_{\nu>} \quad (6.1)$$

Due to viscosity, evolution of energy density (or temperature) is slowed down.

In Fig.3 and 4, we have shown the contour plot of the fluid velocity, v_x and v_y , after evolution of 8.6 fm. As before the black lines are for the ideal fluid evolution. The red and blue lines are for viscous fluid with $\eta/s=0.08$ and 0.135 respectively. Fluid velocities in viscous and ideal fluid differ very little. Even at late time, as shown in Fig.3 and 3, we find that for $\eta/s=0.08-0.135$, x and y component of the fluid velocity show marginal difference. However, there is an indication that in a viscous fluid, velocity grow faster than in ideal fluid. But as mentioned earlier, the difference is marginal.

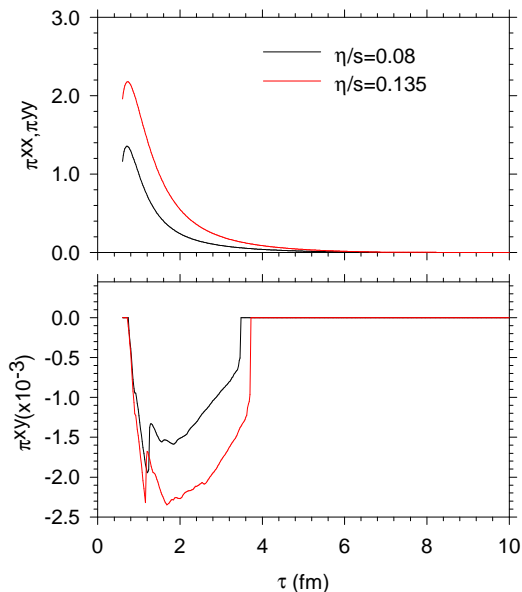


FIG. 7: (color online). In the upper panel, temporal evolution of the shear pressure tensor π^{xx} at the fluid cell $x=y=0$ is shown. In the lower panel, evolution of π^{xy} at the fluid cell $x=y=5$ fm is shown. The black and red lines are for ADS/CFT motivated viscosity $\eta/s=0.08$ and perturbative estimate $\eta/s=0.135$ respectively.

As seen in Fig.1-2, in viscous dynamics, QGP fluid evolves slowly. Thus life-time of the QGP phase is enhanced in viscous dynamics. To obtain an idea about the enhanced life-time, in Fig.5, we have shown the constant temperature contours in $\tau - x$ plane, at a fixed value of $y=0$ fm. As seen in Fig.5, temperature evolves slowly in a viscous fluid and life-time of the QGP phase is extended. For small viscosity $\eta/s=0.08-0.135$, the increase is not large. At the center of the fluid, for $\eta/s=0.135$, QGP life-time is increased approximately by 5% only. It is even less for the ADS/CFT estimate of viscosity. However, enhancement of QGP life-time depends on the fluid

cell position. It could be more. In Fig.6, constant temperature contours at $y=5$ fm is shown. For $\eta/s=0.135$, at $x=0, y=5$ fm, the QGP life-time is enhanced by $\sim 10\%$. We conclude that in a viscous dynamics, with moderate viscosity $\eta/s=0.08-0.135$, QGP life-time could be enhanced by 5-10%. Enhanced lifetime of QGP in a viscous fluid can have significant effect on observables produced early in the collisions e.g. direct photon production or in J/ψ suppression.

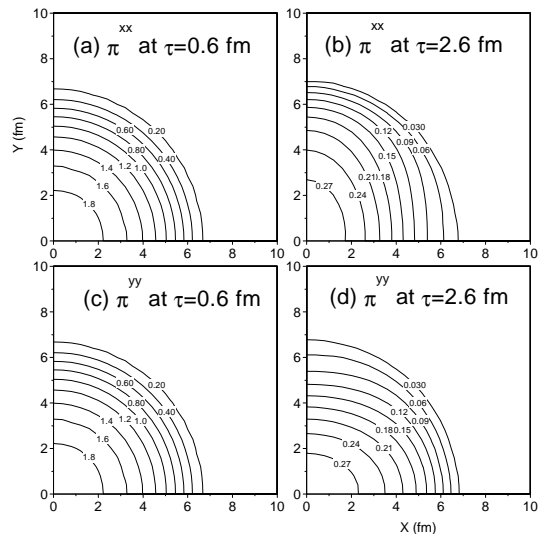


FIG. 8: (color online). In panel (a) and (b), contours of constant pressure tensor π^{xx} at initial time $\tau_i=0.6$ fm and at time $\tau=2.6$ fm is shown. In panel (c) and (d) same results for shear pressure tensor π^{yy} is shown.

B. Evolution of shear pressure tensors

We have assumed that initially the shear pressure tensors π^{xx} , π^{yy} and π^{xy} attained their longitudinal boost-invariant values. As the fluid evolve, pressure tensors also evolve. Here we investigate the evolution of shear pressure tensors with time. In the top panel of Fig.7 evolution of shear pressure tensor π^{xx} at the fluid cell position $x=y=0$ is shown. The black line is for the ADS/CFT motivated viscosity, $\eta/s=0.08$ and the red line is for the perturbative estimate of viscosity $\eta/s=0.135$. Just after the start of the evolution the shear pressure tensor π^{xx} increases, but for a short duration and then steadily decreases with time. By 4 fm of evolution, π^{xx} at the center of the fluid reduces to negligibly small values. Identical behavior is seen for the shear pressure tensor π^{yy} . In the bottom panel of Fig.7 we have shown the evolution of the third independent shear pressure tensor π^{xy} . Initially π^{xy} is zero. As the fluid evolve, it grow in the negative direction. We find that at the centre of the fluid

($x=y=0$), it never grows. In Fig.7, temporal evolution of π^{xy} at the fluid cell position $x = y = 5\text{ fm}$ is shown. From the initial zero value, π^{xy} rapidly increases in the negative direction. It reaches its maximum around $\tau \approx 1$ fm and then decreases again. We also note that π^{xy} never grows to large values. Compared to π^{xx} or π^{yy} stress tensor π^{xy} is negligible. The results indicate that in a QGP fluid, viscous effect persist for a short duration (3-4 fm) only. At late time the fluid evolve essentially as an ideal fluid. The result is understandable. Shear viscosity depend strongly on temperature ($\eta \propto T^3$). As the fluid cools, effect of viscosity decreases rapidly.

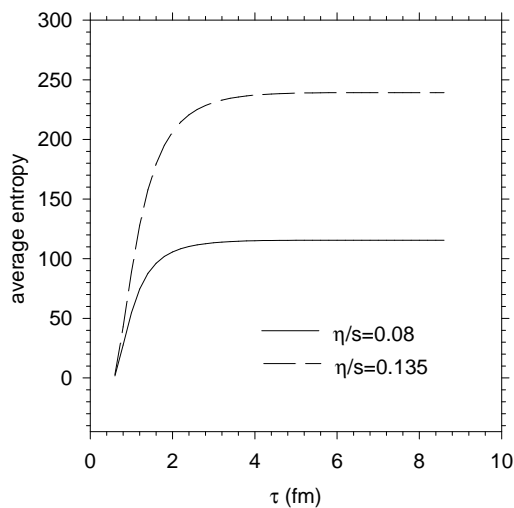


FIG. 9: Evolution of average entropy with time, for two values of viscosity, the ADS/CFT motivated viscosity $\eta/s=0.08$ and perturbative estimate $\eta/s=0.135$ are shown.

To show the spatial distribution of the stress tensors, in Fig.8, π^{xx} and π^{yy} at initial time $\tau_i=0.6$ fm and after an evolution of $\tau = 2.6$ fm are shown. As shown earlier, π^{xx} and also π^{yy} rapidly decreases with time. By 2 fm of evolution they are reduced by approximately by a factor 6. It is also interesting to note that the initial x-y symmetric distribution of π^{xx} and π^{yy} quickly evolves to asymmetric distribution. With time π^{xx} evolves faster in the x-direction than in y-direction. Similarly, π^{yy} evolve faster in the y-direction than in the x-direction. For central collisions the asymmetric evolution of π^{xx} and π^{yy} counter balance each other. As shown in Fig.1 and 2, the contour plots of energy density do not show any indication of asymmetry even at late time. However, the asymmetric pressure tensors can have important effects on elliptic flow of observables produced early in the collisions, say in elliptic flow of direct photons.

C. Entropy generation

In a viscous fluid dynamics, entropy is generated. We can easily calculate the entropy generated during the evolution,

$$\begin{aligned} \partial_\mu S^\mu &= \frac{\pi^{\mu\nu} \pi_{\mu\nu}}{2\eta T} \\ &= \frac{1}{2\eta T} [(\pi^{\tau\tau})^2 + (\pi^{xx})^2 + (\pi^{yy})^2 + (\tau^2 \pi^{\eta\eta})^2 \\ &\quad - 2(\pi^{\tau x})^2 - 2(\pi^{\tau y})^2 + 2(\pi^{xy})^2] \end{aligned} \quad (6.2)$$

Evolution of spatially averaged entropy is shown in Fig.9, for the two values of viscosity coefficients $\eta/s=0.08$ and 0.135. As expected, entropy generation is more if viscosity is more. For both the values of viscosity, we find that entropy generation saturates after ≈ 3 fm of evolution. It is expected also. As shown previously, viscous fluxes reduces to very small values after $\tau=3$ fm. Naturally, entropy generation is negligible thereafter.

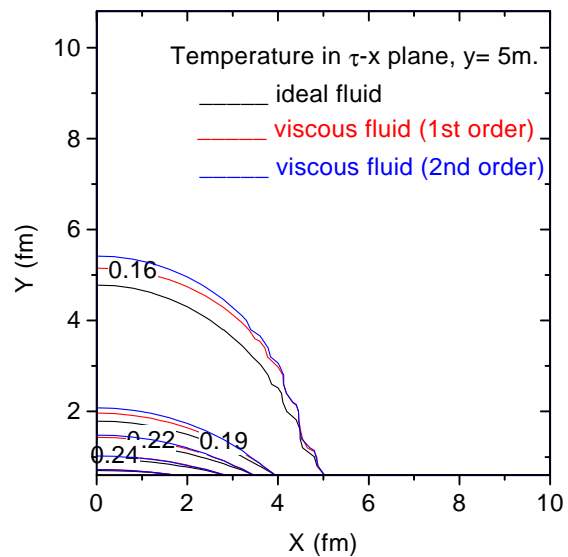


FIG. 10: (color online) constant temperature contours in $x - \tau$ plane at $y=5$ fm. The black lines are for ideal fluid. The red and blue lines are for viscous fluid in 1st order and in 2nd order theory respectively. $\eta/s=0.135$.

D. 1st order theory vs. 2nd order theory

As mentioned earlier, 1st order theory of dissipative hydrodynamics is acausal, signal can travel faster than light. This is corrected in 2nd order theory, but we have to pay the price, relaxation equations for dissipative fluxes are required to be solved. It is interesting to

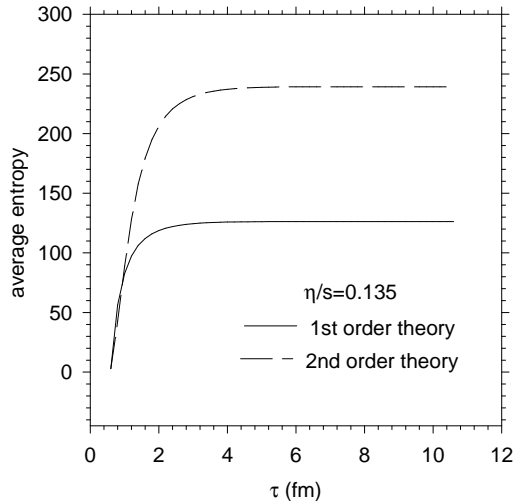


FIG. 11: Evolution of average entropy production in a 1st order (solid line) and 2nd order (dashed line) theory. 2nd order theory generate more entropy.

compare the difference we can expect in a first order theory and in a 2nd order theory of dissipation. In Fig. 10, we have shown the contours of constant temperature in $x-\tau$, for a fixed $y = 5fm$. The black lines are for an ideal fluid. The red lines are for a viscous fluid treated in the 1st order theory. The blue lines are for viscous fluid in 2nd order theory. In 2nd order theory fluid evolve more slowly than in a first order theory. Entropy generation is also more in a 2nd order theory. In Fig.11, average entropy evolution with proper time is shown, both for the 1st order theory (the solid line) and the 2nd order theory. In 2nd order theory, approximately 80% more entropy is generated.

VII. TRANSVERSE MOMENTUM AND ELLIPTIC FLOW OF QUARKS

Presently we can not compare predictions from viscous hydrodynamics with experimental data. Hadrons are not included in the model. The initial QGP fluid evolve and cools but remain in the QGP phase, it did not undergo a phase transition to hadronic gas. However, from the momentum distribution of quarks we can get some idea about the viscous effect on particle production. Viscosity generates entropy, which will be reflected in enhanced multiplicity. We use the standard Cooper-Frey prescription to obtained the transverse momentum distribution of quarks. In Cooper-Frey prescription, particle distribution is obtained by convoluting the one body distribution function over the freeze-out surface,

$$E \frac{dN}{d^3p} == \int_{\Sigma} d\Sigma_{\mu} p^{\mu} f(x, p) \quad (7.1)$$

where $d\Sigma_{\mu}$ is the freeze-out hyper-surface and $f(x, p)$ is the one-body distribution function. Now in a viscous dynamics, the fluid is not in equilibrium and $f(x, p)$ can not be approximated by the equilibrium distribution function,

$$f^{(0)}(x, p) = \frac{1}{\exp[\beta(u_{\mu} p^{\mu} - \mu)] \pm 1}, \quad (7.2)$$

with inverse temperature $\beta = 1/T$ and chemical potential μ . In a highly non-equilibrium system, distribution function $f(x, p)$ is unknown. If the system is slightly off-equilibrium, then it is possible to calculate correction to equilibrium distribution function due to (small) non-equilibrium effects. Slightly off-equilibrium distribution function can be approximated as,

$$f(x, p) = f^{(0)}(x, p)[1 + \phi(x, p)], \quad (7.3)$$

$\phi(x, p)$ is the deviation from equilibrium distribution function $f^{(0)}$. With shear viscosity as the only dissipative forces, $\phi(x, p)$ can be locally approximated by a quadratic function of 4-momentum,

$$\phi(x, p) = \varepsilon_{\mu\nu} p^{\mu} p^{\nu}. \quad (7.4)$$

Without any loss of generality $\varepsilon_{\mu\nu}$ can be written as,

$$\varepsilon_{\mu\nu} = \frac{1}{2(\varepsilon + p)T^2} \pi^{\mu\nu}, \quad (7.5)$$

completely specifying the non-equilibrium distribution function. As expected, correction factor increases with increasing viscosity. We also note that non-equilibrium correction is more on large momentum particles. The effect of viscosity is more on large momentum particles. The correction factor reduces if freeze-out occurs at higher temperature.

With the corrected distribution function, we can calculate the quark momentum spectra at freeze-out surface Σ_{μ} . In appendix D, relevant equations are given. The quark momentum distribution has two parts, (i) $\frac{dN^{eq}}{dyd^2p_T}$, obtained by convoluting the equilibrium distribution function over the freeze-out surface and (ii) $\frac{dN^{neq}}{dyd^2p_T}$, obtained by convoluting the correction to the equilibrium distribution function over the freeze-out surface. Since the correction factor is obtained under the assumption that non-equilibrium effects are small, $\phi(x, p) \ll 1$, it necessarily imply that, $\frac{dN^{neq}}{dyd^2p_T} \ll \frac{dN^{eq}}{dyd^2p_T}$. The ratio,

$$\frac{dN^{neq}}{dN^{eq}} = \frac{\frac{dN^{neq}}{dyd^2p_T}}{\frac{dN^{eq}}{dyd^2p_T}}, \quad (7.6)$$

could at best be unity or less. If the ratio exceeds unity, it will imply that non-equilibrium effects are large

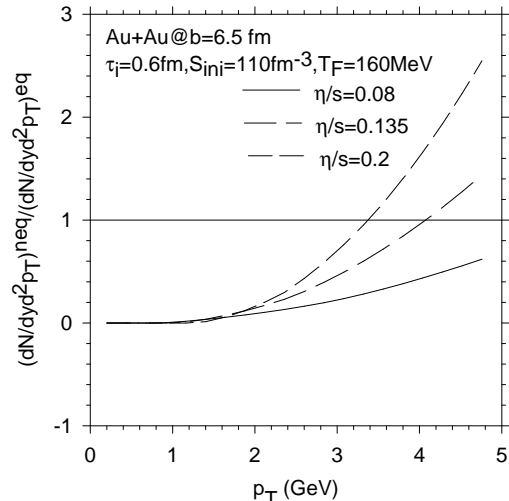


FIG. 12: Ratio of quark spectra with non-equilibrium distribution function to that with equilibrium distribution function.

and the distribution function $f(x, p)$ can not be approximated as in Eq.7.3. Using AZHYDRO-KOLKATA, we have simulated a $b=6.5$ fm Au+Au collision. $\frac{dN^{eq}}{dyd^2p_T}$ and $\frac{dN^{neq}}{dyd^2p_T}$ at freeze-out temperature $T_F=160$ MeV are calculated. The ratio $\frac{dN^{neq}}{dN^{eq}}$ for $\eta/s=0.08, 0.135$ and 0.2 , are shown in Fig.12. With ADS/CFT estimate of viscosity, $\eta/s=0.08$, non-equilibrium correction to particle production become comparable to equilibrium contribution only beyond $p_T=5$ GeV. However, with perturbative estimate, $\eta/s=0.135$, non-equilibrium correction become comparable to or exceeds the equilibrium contribution at $p_T \sim 4$ GeV. p_T range is further reduced for higher viscosity $\eta/s=0.2$. Thus with perturbative estimate of viscosity ($\eta/s = 0.135 - 0.2$), hydrodynamic description remain valid upto transverse momentum $p_T \sim 3.5-4$ GeV.

In Fig.13, we have compared the transverse momentum spectra of quarks in ideal hydrodynamics with that in a viscous dynamics. In Fig.13, the dotted line is the spectra obtained in ideal dynamics ($\eta/s = 0$). The p_T spectra in viscous dynamics are shown by black lines. We have shown the spectra for three values of viscosity $\eta/s=0.08, 0.135$ and 0.2 . Compared to ideal dynamics, quarks yield in viscous dynamics increases. The increase is more at large p_T . For low values of viscosity the increase is modest, a factor of 2 at $p_T=3$ GeV. But yield increase by a factor or 4(10) if viscosity increases to $\eta/s=0.135$ (2). Please note that even though we have shown p_T spectra upto 5 GeV, for $\eta/s=0.2$ and 0.135 , hydrodynamic description fails beyond $p_T \sim 3.5$ and 4 GeV.

We have also studied the effect of viscosity on quark elliptic flow. Effect of viscosity is very prominent on elliptic flow. In Fig.14, p_T dependence of elliptic flow of quarks, in a $b=6.5$ fm collision is shown. The black line is v_2 in ideal dynamics. In ideal dynamics, ellip-

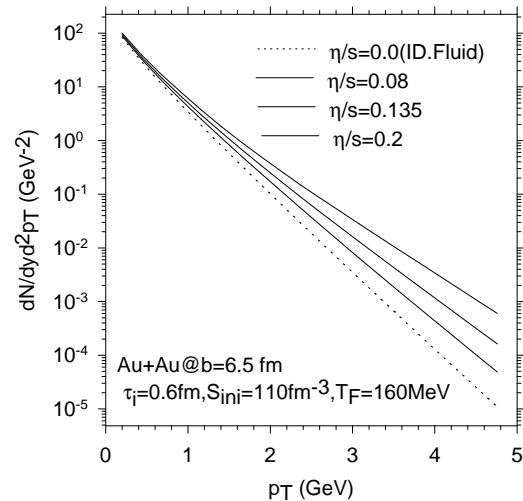


FIG. 13: Quark transverse momentum spectra at freeze-out temperature of 160 MeV. The dotted line is the quarks spectra in ideal hydrodynamics. The solid lines (top to bottom) are in viscous dynamics with $\eta/s=0.08, 0.135$ and 0.2 .

tic flow continually increases with p_T . It well known, in contrast to experiments, where elliptic flow saturates at large p_T , in ideal hydrodynamics, elliptic flow continue to increase with p_T . Indeed, this is a major problem in ideal hydrodynamics. The renewed the interest in dissipative hydrodynamics is partly due to the inability of ideal hydrodynamics to predict the trend of elliptic flow in Au+Au collisions. In Fig.14, the blue lines are v_2 in viscous dynamics with $\eta/s=0.08, 0.135$ and 0.2 respectively. In a viscous dynamics, p_T dependence of v_2 is drastically changed. In contrast to ideal dynamics where v_2 continue to increase with p_T , in viscous dynamics, v_2 continue to increase only upto $p_T \sim 1.5 - 2$ GeV. Thereafter v_2 decreases. For perturbative estimate of viscosity $\eta/s=0.135$ and beyond, v_2 even become negative at large p_T . Veering about of v_2 after $p_T \sim 1.5-2$ GeV is due to viscous effect only or more explicitly due to the non-equilibrium correction to the equilibrium distribution function. This is clearly manifested from the red lines in Fig.14. The red lines are calculated ignoring the non-equilibrium corrections to the equilibrium distribution function. If non-equilibrium correction is ignored, in viscous dynamics also, v_2 continue to increase with p_T , albeit its magnitude is reduced compared to ideal dynamics. The result is very important. It imply that the experimental trend of elliptic flow (saturation at large p_T) could only be explained if the QGP fluid is viscous. An ideal QGP, will not be able to explain the saturation trend of the experimental data.

As stated earlier, non-equilibrium correction to the equilibrium distribution function depends on the freeze-out condition. To show the effect of freeze-out condition, on v_2 , in Fig.15 we have shown v_2 for a values of freeze-out temperature $T_F = 160, 150, 140, 130$ and 120 MeV. As

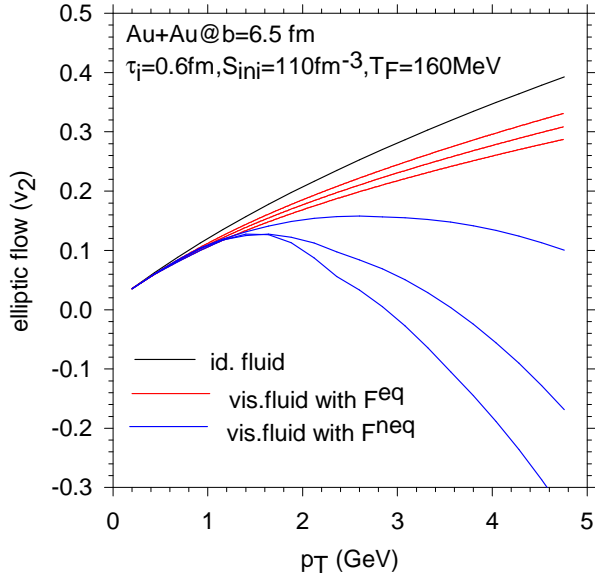


FIG. 14: (color online) Elliptic flow as a function of transverse momentum. The black line is v_2 in ideal hydrodynamics. The blue lines are v_2 in viscous dynamics with viscosity to entropy ratio $\eta/s=0.08, 0.135$ and 0.2 (top to bottom) respectively, including the correction to equilibrium distribution function. The red lines are same as the blues lines but ignoring the non-equilibrium correction to the distribution function.

freeze-out occur at higher and higher temperature, the veering of v_2 takes place at larger and larger p_T and for $T_F=120$ MeV, the elliptic flow saturates. The result is understood easily. With decreasing freeze-out temperature, the fluid evolves for longer time, the shear stress-tensor's at the freeze-out surface is reduced and the non-equilibrium correction, proportional to shear stress tensors, decreases.

VIII. STABILITY OF NUMERICAL SOLUTIONS IN AZHYDRO-KOLKATA

Before we summarise our results, we would like to comment on the stability of numerical solutions in AZHYDRO-KOLKATA. As indicated above, with shear viscosity as the only dissipative force, boost-invariant causal hydrodynamics require simultaneous solution of six partial differential equations. Numerical solution of six partial differential equations is non-trivial and it is important to check for the numerical stability of the solutions. Analytical solutions of viscous hydrodynamics, even in restrictive conditions are not available, and we can not check the solutions against analytical results. However, we can check for the stability of the numerical solutions. The standard procedure of checking the numerical stability is to change the integration step lengths and look for the difference in the solution. In Fig.16, for viscosity $\eta/s=0.135$, we have shown the constant temperature contours in $x - \tau$ plane at a fixed

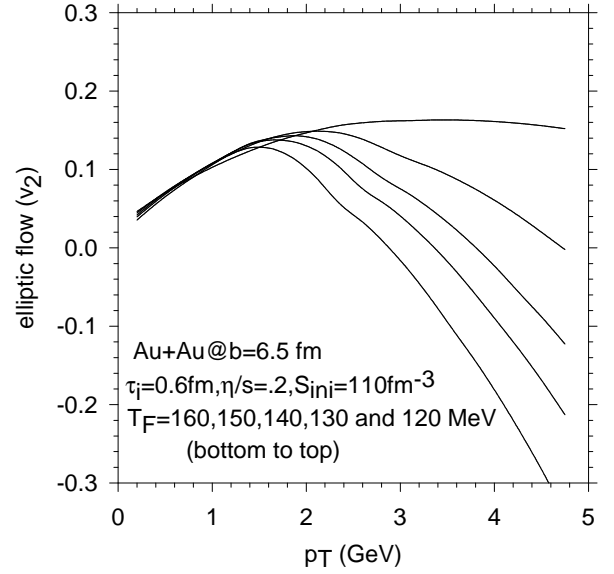


FIG. 15: Dependence of elliptic flow on the freeze-out temperature. The solid lines (from bottom to top) are elliptic flow (v_2) in viscous dynamics with $T_F=160, 150, 140, 130$ and 120 MeV respectively.

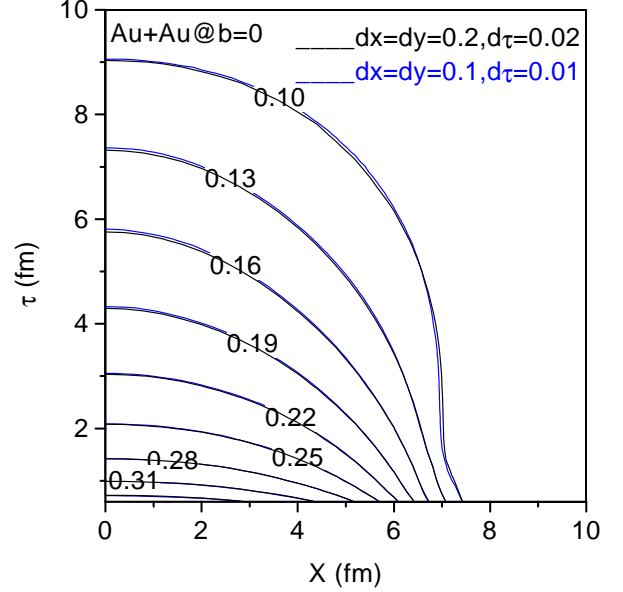


FIG. 16: (color online) constant temperature contours in $x - \tau$ plane at a fixed $y=0$ fm. The black lines are obtained with integration step lengths $dx=dy=0.2$ fm and $d\tau=0.02$ fm. The blue lines are obtained with integration step lengths, $dx=dy=0.1$ fm and $d\tau=0.01$ fm. Halving the step lengths do not change the evolution. The numerical solutions are stable.

$y=0$ fm. The black and blue lines are obtained when integration step lengths are $dx=dy=0.2$ fm, $d\tau=0.02$ fm, and $dx=dy=0.1$ fm, $d\tau=0.01$ fm respectively. Evolution of QGP fluid do not alter by changing the step lengths, the solutions are stable against mesh size.

IX. SUMMARY AND CONCLUSIONS

In Israel-Stewart's 2nd order theory of dissipative relativistic hydrodynamics, we have studied evolution QGP fluid. In 2nd order theory, in addition to usual thermodynamic quantities e.g. energy density, pressure, hydrodynamic velocities, dissipative flows are treated as extended thermodynamic variables. Relaxation equations for dissipative flows are solved, simultaneously with the energy-momentum conservation equations. This greatly enhances the complexity of the problem. Altogether 14 partial differential equations are required to be solved. We simplify the problem to solution of six partial differential equations by considering the evolution of baryon free QGP fluid with longitudinal boost-invariance. We also consider dissipation due to shear viscosity only, disregarding the bulk viscosity and the heat conduction (for a baryon free QGP fluid they do not contribute). The six partial differential equations are solved using the code AZHYDRO-KOLKATA, developed at the Cyclotron Centre, Kolkata.

To bring out the effect of viscosity, we have considered the evolution of ideal as well as viscous QGP fluid. Both ideal and viscous fluid are initialized similarly, at initial time $\tau_i=0.6$ fm, the central entropy density is 110 fm^{-3} . Viscous dynamics require initial conditions for the shear stress tensor components. It is assumed that at the equilibration time, the shear stress tensors components have attained their boost-invariant values.

Explicit simulation of ideal and viscous fluids confirms that energy density of a viscous fluid, evolve slowly than its ideal counterpart. Thus in a viscous fluid, lifetime of the QGP phase will be enhanced. Transverse expansion is also more in viscous dynamics. For a similar freeze-out condition freeze-out surface is extended in viscous fluid.

As the fluid evolve, shear pressure tensors also evolve. Explicit simulations indicate that shear pressure tensors π^{xx} and π^{yy} which are initially non zero, rapidly decreases as the fluid evolve. By 3-4 fm of evolution they reduced to very small values. The other independent shear tensor π^{xy} is zero initially. At later time it grow in the negative direction but never grow to large value and is always order of magnitude smaller than the stress tensors (π^{xx} and π^{yy}). Spatial distribution of shear pressure tensors π^{xx} and π^{yy} reveal an interesting feature of viscous dynamics. Initially π^{xx} and π^{yy} have symmetric distribution. As the fluid evolve, pressure tensors quickly become asymmetric, e.g. π^{xx} evolve faster in the x-direction than in the y-direction, π^{yy} evolve faster in y direction than in x-direction. However, in a central collision, we did not see any effect of asymmetry in the energy density distribution. In a central b=0 collision, the two opposite asymmetry cancels each other.

We could not study effect of shear viscosity on particle production. However, we have explored the effect of viscosity on parton momentum distribution and elliptic flow. We have simulated b=6.5 fm Au+Au collision. Using the Cooper-Frey prescription, transverse momen-

tum spectra as well as elliptic flow of quarks at freeze-out temperature of $T_F=160$ MeV are obtained. Viscous dynamics flattens the quark yield at large p_T . At $p_T=3$ GeV, even a small viscosity, $\eta/s=0.8$, increase the yield by a factor of 2. The increase is even more if viscosity is large. Viscous effect is most prominent on elliptic flow. In ideal hydrodynamics, elliptic flow continue to increase with p_T . But in viscous dynamics v_2 veer about around $p_T=1.5-2$ and even become negative at large p_T . With appropriate choice of viscosity, freeze-out condition, elliptic flow show saturation. The saturation effect is essentially due to non-equilibrium correction to the equilibrium distribution function and can not be mimicked in an ideal hydrodynamics. Only in viscous dynamics, saturation of elliptic flow can be explained.

APPENDIX A: COORDINATE TRANSFORMATIONS

Instead of Cartesian coordinates $x^\mu = (t, x, y, z)$ we use curvilinear coordinates in longitudinal proper time and rapidity, $\bar{x}^m = (\tau, x, y, \eta)$:

$$t = \tau \cosh \eta; \quad \tau = \sqrt{t^2 - z^2} \quad (\text{A1})$$

$$z = \tau \sinh \eta; \quad \eta = \frac{1}{2} \ln \frac{t+z}{t-z}. \quad (\text{A2})$$

The differentials

$$dt = d\tau \cosh \eta + d\eta \tau \sinh \eta, \quad (\text{A3})$$

$$dz = d\tau \sinh \eta + d\eta \tau \cosh \eta, \quad (\text{A4})$$

and the metric tensor is easily read off from

$$\begin{aligned} ds^2 &= g_{\mu\nu} dx^\mu dx^\nu = dt^2 - dx^2 - dy^2 - dz^2 \\ &= \bar{g}_{mn} d\bar{x}^m d\bar{x}^n = d\tau^2 - dx^2 - y^2 - \tau^2 d\eta^2, \end{aligned} \quad (\text{A5})$$

namely

$$\bar{g}_{mn} = \begin{pmatrix} 1 & 0 & 0 & 0 \\ 0 & -1 & 0 & 0 \\ 0 & 0 & -1 & 0 \\ 0 & 0 & 0 & -\tau^2 \end{pmatrix}, \quad \bar{g}^{mn} = \begin{pmatrix} 1 & 0 & 0 & 0 \\ 0 & -1 & 0 & 0 \\ 0 & 0 & -1 & 0 \\ 0 & 0 & 0 & -1/\tau^2 \end{pmatrix} \quad (\text{A6})$$

In curvilinear coordinates we must replace the partial derivatives with respect to x^μ by covariant derivatives (denoted by a semicolon) with respect to \bar{x}^m :

$$\bar{T}^i{}_{;p}{}^k = \frac{\partial \bar{T}^{ik}}{\partial \bar{x}^p} + \Gamma_{pm}^i \bar{T}^{mk} + \bar{T}^{im} \Gamma_{mp}^k.$$

The only non-vanishing Christoffel symbols are

$$\Gamma_{\eta\eta}^\tau = \tau; \quad \Gamma_{\tau\eta}^\eta = \Gamma_{\eta\tau}^\eta = 1/\tau. \quad (\text{A7})$$

The hydrodynamic 4-velocity $u^\mu = \gamma(1, v_x, v_y, v_z)$ is transformed to $\bar{u}^m = \gamma(1, v_x, v_y, 0)$, with $\gamma_\perp = 1/\sqrt{1-v_r^2}$. From here on, we drop the bars over tensor components in \bar{x} -coordinates for simplicity.

The projector can be easily calculated,

$$\begin{aligned} \Delta^{\mu\nu} &= g^{\mu\nu} - u^\mu u^\nu \\ &= \begin{pmatrix} 1 - \gamma_\perp^2 & -\gamma_\perp^2 v_x & \gamma_\perp^2 v_y & 0 \\ -\gamma_\perp^2 v_x & -1 - \gamma_\perp^2 v_x^2 & -\gamma_\perp^2 v_x v_y & 0 \\ -\gamma_\perp^2 v_y & -\gamma_\perp^2 v_x v_y & -1 - \gamma_\perp^2 v_y^2 & 0 \\ 0 & 0 & 0 & \frac{1}{\tau^2} \end{pmatrix} \end{aligned} \quad (\text{A8})$$

In (τ, x, y, η) coordinate system, the convective time derivative can be obtained as,

$$D = u \cdot \partial = \gamma(\partial_\tau + v_x \partial_x + v_y \partial_y). \quad (\text{A9})$$

For future reference, we also write down the the scalar expansion rate

$$\theta = \partial \cdot u = \partial_\tau u^\tau + \partial_x u^x + \partial_y u^y + \frac{u^\tau}{\tau} \quad (\text{A10})$$

APPENDIX B: ENERGY-MOMENTUM CONSERVATION

With longitudinal boost-invariance the energy-momentum conservation equations $T^{mn}{}_{;n} = 0$ yield

$$\partial_\tau \tilde{T}^{\tau\tau} + \partial_x (\tilde{T}^{\tau\tau} \bar{v}_x) + \partial_y (\tilde{T}^{\tau\tau} \bar{v}_y) = -(p + \tau^2 \pi^{\eta\eta}) \quad (\text{B1})$$

$$\partial_\tau \tilde{T}^{\tau x} + \partial_x (\tilde{T}^{\tau x} v_x) + \partial_y (\tilde{T}^{\tau x} v_y) = -\partial_x (\tilde{p} + \tilde{\pi}^{xx} - \tilde{\pi}^{\tau x} v_x) - \partial_y (\tilde{\pi}^{xy} - \tilde{\pi}^{\tau x} v_y) \quad (\text{B2})$$

$$\partial_\tau \tilde{T}^{\tau y} + \partial_x (\tilde{T}^{\tau y} v_x) + \partial_y (\tilde{T}^{\tau y} v_y) = -\partial_x (\tilde{\pi}^{xy} - \tilde{\pi}^{\tau y} v_x) - \partial_y (\tilde{p} + \tilde{\pi}^{yy} - \tilde{\pi}^{\tau y} v_y) \quad (\text{B3})$$

where $\tilde{A}^{mn} \equiv \tau A^{mn}$, $\tilde{p} \equiv \tau p$, and $\bar{v}_x \equiv T^{\tau x}/T^{\tau\tau}$, $\bar{v}_y \equiv T^{\tau y}/T^{\tau\tau}$.

The components of the energy momentum tensors, including the shear pressure tensor are,

$$T^{\tau\tau} = (\varepsilon + p)\gamma_\perp^2 - p + \pi^{\tau\tau} \quad (\text{B4})$$

$$T^{\tau x} = (\varepsilon + p)\gamma_\perp^2 v_x + \pi^{\tau x} \quad (\text{B5})$$

$$T^{\tau y} = (\varepsilon + p)\gamma_\perp^2 v_y + \pi^{\tau y} \quad (\text{B6})$$

In causal dissipative hydrodynamics, energy momentum conservation equations are solved simultaneously with the relaxation equations. Given an equation of state, if energy density (ε) and fluid velocity (v_x and v_y) distributions, at any time τ_i are known, Eqs.B1,B2 and B3 can be integrated to obtain ε , v_x and v_y at the next time step τ_{i+1} . While for ideal hydrodynamics, this procedure works perfectly, viscous hydrodynamics poses a problem that shear stress-tensor components contains time derivatives, $\partial_\tau \gamma_\perp$, $\partial_\tau u^x$, $\partial_\tau u^y$ etc. Thus at time step τ_i one needs the still unknown time derivatives. Numerically, time derivatives at step τ_i could be obtained if velocities at time step τ_i and τ_{i+1} are known. One possible way to circumvent the problem, is to use time derivatives of the previous step, i.e. use velocities at time step τ_{i-1} and τ_i to calculate the derivatives at time step τ_i [18]. The underlying assumption that fluid velocity changes slowly with time. In 1st order theories, this problem is circumvented by calculating the time derivatives from the ideal equation of motion ,

$$Du^\mu = \frac{\nabla^\mu p}{\varepsilon + p}, \quad (\text{B7})$$

$$D\varepsilon = -(\varepsilon + p)\nabla_\mu u^\mu. \quad (\text{B8})$$

With the help of these two equations all the time derivatives can be expressed entirely in terms of spatial gradients [15, 26]. 1st order theories are restricted to contain terms at most linear in dissipative quantities. Neglect of viscous terms can contribute only in 2nd order corrections, which are neglected in 1st order theories. While the procedure is not correct in 2nd order theory, we still use it in the present calculations. The alternative procedure of using the derivative of earlier time step is not correct either.

APPENDIX C: RELAXATION EQUATIONS FOR THE VISCOUS PRESSURE TENSOR

Being symmetric and traceless, the viscous pressure tensor $\pi^{\mu\nu}$ has 9 independent components. The assumption of boost invariance reduces this number by 3 ($\nabla^{(m} u^{\eta)} = 0$, $m \neq \eta$). The transversality condition $u_m \pi^{mn} = 0$ eliminates another three components (u_η vanish and thus yield no constraint). Thus, with boost-invariance the viscous pressure tensor has only three independent components. As seen in Eqs.B1,B2 and B3 in a boost-invariant evolution only seven pressure tensors $\pi^{\tau\tau}$, π^{xx} , π^{yy} , $\pi^{\eta\eta}$, $\pi^{\tau x}$, $\pi^{\tau y}$ and π^{xy} are of importance. Only three of these seven are independent. In an earlier publication [17], we have debated about the choice of the independent components and suggested use of either ($\pi^{\tau\tau}$, $\pi^{\eta\eta}$, $\Delta = \pi^{xx} - \pi^{yy}$) or ($\pi^{\tau\tau}$, $\pi^{\eta\eta}$, $\pi^{\tau x}$, $\pi^{\tau y}$) (which will require solution of an additional relaxation equation) as choice of independent components. However, while computing we find that the three pressure tensors π^{xx} and π^{yy} and π^{xy} as independent components are computationally more convenient. The choice has the advantage that the dependent shear stress tensors can be obtained from the 3 independent stress tensors by

multiplying them by fluid velocity, v_x and v_y (see Eqs. C7-C10). In any other choice of independent components (e.g. $\pi^{\tau\tau}, \pi^{\eta\eta}, \Delta = \pi^{xx} - \pi^{yy}$), the evaluation of dependent stress tensors requires division by fluid velocities. Since initially, fluid velocities are assumed to be zero and they grow slowly, these choices will involve division by very small numbers. Unless proper care is not taken, di-

vision by small numbers can lead to unrealistically large values for the dependent stress tensors and ruin the computation.

The relaxation equations for the independent shear stress tensors π^{xx} , π^{yy} and π^{xy} , in (τ, x, y, η) co-ordinate can be written as,

$$\partial_\tau \pi^{xx} + v_x \partial_x \pi^{xx} + v_y \partial_y \pi^{xx} = -\frac{1}{\tau_\pi \gamma} (\pi^{xx} - 2\eta \sigma^{xx}) \quad (C1)$$

$$\partial_\tau \pi^{yy} + v_x \partial_x \pi^{yy} + v_y \partial_y \pi^{yy} = -\frac{1}{\tau_\pi \gamma} (\pi^{yy} - 2\eta \sigma^{yy}) \quad (C2)$$

$$\partial_\tau \pi^{xy} + v_x \partial_x \pi^{xy} + v_y \partial_y \pi^{xy} = -\frac{1}{\tau_\pi \gamma} (\pi^{xy} - 2\eta \sigma^{xy}) \quad (C3)$$

where τ_π is the relaxation time, $\tau_\pi = 2\eta\beta_2$ (see Eq.2.21). In ultra-relativistic limit, for a Boltzman gas, β_2 can be evaluated, $\beta_2 \approx \frac{3}{4p}$ where p is the pressure [13]. In the present paper, we use this limit to obtain the relaxation time τ_π .

The viscous pressure tensor relaxes on a time scale τ_π to 2η times the shear tensor $\sigma^{\mu\nu} = \nabla^{(\mu} u^{\nu)}$. The xx , yy and xy components of the shear tensor $\sigma^{\mu\nu}$ can be written as

$$\sigma^{xx} = -\partial_x u^x - u^x D u^x - \frac{1}{3} \Delta^{xx} \theta \quad (C4)$$

$$\sigma^{yy} = -\partial_y u^y - u^y D u^y - \frac{1}{3} \Delta^{yy} \theta \quad (C5)$$

$$\begin{aligned} \sigma^{xy} = & -\frac{1}{2} [\partial_x u^y - \partial_y u^x - u^x D u^y - u^y D u^x] \\ & - \frac{1}{3} \Delta^{xy} \theta \end{aligned} \quad (C6)$$

The dependent shear stress tensors can easily be obtained from the independent ones as,

$$\pi^{\tau x} = v_x \pi^{xx} + v_y \pi^{xy} \quad (C7)$$

$$\pi^{\tau y} = v_x \pi^{xy} + v_y \pi^{yy} \quad (C8)$$

$$\pi^{\tau\tau} = v_x^2 \pi^{xx} + v_y^2 \pi^{yy} + 2v_x v_y \pi^{xy} \quad (C9)$$

$$\begin{aligned} \tau^2 \pi^{\eta\eta} = & -(1 - v_x^2) \pi^{xx} - (1 - v_y^2) \pi^{yy} \\ & + 2v_x v_y \pi^{xy} \end{aligned} \quad (C10)$$

The expressions for the convective time derivative D and expansion scalar $\theta = \partial \dot{u}$, in (τ, x, y, η) are given in Eqs. A9 and A10.

APPENDIX D: PARTICLE SPECTRA

With the non-equilibrium distribution function thus specified, it can be used to calculate the particle spectra

from the freeze-out surface. In the standard Cooper-Frye prescription, particle distribution is obtained as,

$$E \frac{dN}{d^3p} = \frac{dN}{dy d^2p_T} = \int_\Sigma d\Sigma_\mu p^\mu f(x, p) \quad (D1)$$

In (τ, x, y, η_s) coordinate, the freeze-out surface is parameterised as,

$$\Sigma^\mu = (\tau_f(x, y) \cosh \eta_s, x, y, \tau_f(x, y) \sinh \eta_s), \quad (D2)$$

and the normal vector on the hyper surface is,

$$d\Sigma_\mu = (\cosh \eta_s, -\frac{\partial \tau_f}{\partial x_f}, -\frac{\partial \tau_f}{\partial y_f}, -\sinh \eta_s) \tau_f dx dy d\eta_s \quad (D3)$$

At the fluid position (τ, x, y, η_s) the particle 4-momenta are parameterised as,

$$p^\mu = (m_T \cosh(\eta_s - Y), p^x, p^y, m_T \sinh(\eta_s - Y)) \quad (D4)$$

The volume element $p^\mu d\Sigma_\mu$ become,

$$p^\mu d\Sigma_\mu = (m_T \cosh(\eta - Y) - \vec{p}_T \cdot \vec{\nabla}_T \tau_f) \tau_f dx dy d\eta \quad (D5)$$

Equilibrium distribution function involve the term $\frac{p^\mu u_\mu}{T}$ which can be evaluated as,

$$\frac{p^\mu u_\mu}{T} = \frac{\gamma(m_T \cosh(\eta - Y) - \vec{v}_T \cdot \vec{p}_T - \mu/\gamma)}{T} \quad (D6)$$

The non-equilibrium distribution function require the sum $p^\mu p^\nu \pi_{\mu\nu}$,

$$p_\mu p_\nu \pi^{\mu\nu} = a_1 \cosh^2(\eta - Y) + a_2 \cosh(\eta - Y) + a_3 \quad (D7)$$

with

$$a_1 = m_T^2(\pi^{\tau\tau} + \tau^2\pi^{\eta\eta}) \quad (\text{D8})$$

$$a_2 = -2m_T(p_x\pi^{\tau x} + p_y\pi^{\tau y}) \quad (\text{D9})$$

$$a_3 = p_x^2\pi^{xx} + p_y^2\pi^{yy} + 2p_xp_y\pi^{xy} - m_T^2\tau^2\pi^{\eta\eta} \quad (\text{D10})$$

Inserting all the relevant formulas in Eq.D1 and inte-

grating over spatial rapidity one obtains,

$$\frac{dN}{dyd^2p_T} = \frac{dN^{eq}}{dyd^2p_T} + \frac{dN^{neq}}{dyd^2p_T} \quad (\text{D11})$$

with,

$$\frac{dN^{eq}}{dyd^2p_T} = \frac{g}{(2\pi)^3} \int dx dy \tau_f [m_T K_1(n\beta) - p_T \vec{\nabla}_T \tau_f K_0(n\beta)] \quad (\text{D12})$$

$$\begin{aligned} \frac{dN^{neq}}{dyd^2p_T} = \frac{g}{(2\pi)^3} \int dx dy \tau_f [m_T \{ \frac{a_1}{4} K_3(n\beta) + \frac{a_2}{2} K_2(n\beta) + (\frac{3a_1}{4} + a_3) K_1(n\beta) + \frac{a_2}{2} K_0(n\beta) \} \\ - \vec{p}_T \cdot \vec{\nabla}_T \tau_f \{ \frac{a_1}{2} K_2(n\beta) + a_2 K_1(n\beta) + (\frac{a_1}{2} + a_3) K_0(n\beta) \}] \end{aligned} \quad (\text{D13})$$

where K_0 , K_1 , K_2 and K_3 are the modified Bessel functions.

We will also show results for elliptic flow v_2 . It is defined as,

$$V_2 = \frac{\int_0^{2\pi} \frac{dN}{dyd^2p_T} \cos(2\phi) d\phi}{\int_0^{2\pi} \frac{dN}{dyd^2p_T} d\phi} \quad (\text{D14})$$

Expanding to the 1st order, elliptic flow as a function

of transverse momentum can be obtained as,

$$v_2(p_T) = v_2^{eq}(p_T) \left(1 - \frac{\int d\phi \frac{d^2 N^{neq}}{p_T dp_T d\phi}}{\int d\phi \frac{d^2 N^{eq}}{p_T dp_T d\phi}} \right) + \frac{\int d\phi \cos(2\phi) \frac{d^2 N^{neq}}{p_T dp_T d\phi}}{\int d\phi \frac{d^2 N^{eq}}{p_T dp_T d\phi}} \quad (\text{D15})$$

where v_2^{eq} is the elliptic flow calculated with the equilibrium distribution f^{eq} .

-
- [1] BRAHMS Collaboration, I. Arsene *et al.*, Nucl. Phys. A **757**, 1 (2005).
- [2] PHOBOS Collaboration, B. B. Back *et al.*, Nucl. Phys. A **757**, 28 (2005).
- [3] PHENIX Collaboration, K. Adcox *et al.*, Nucl. Phys. A **757** (2005), in press [arXiv:nucl-ex/0410003].
- [4] STAR Collaboration, J. Adams *et al.*, Nucl. Phys. A **757** (2005), in press [arXiv:nucl-ex/0501009].
- [5] Karsch F, Laermann E, Petreczky P, Stickan S and Wetzorke I, 2001 *Proceedings of NIC Symposium* (Ed. H. Rollnik and D. Wolf, John von Neumann Institute for Computing, Jülich, NIC Series, vol.9, ISBN 3-00-009055-X, pp.173-82,2002.)
- [6] P. F. Kolb and U. Heinz, in *Quark-Gluon Plasma 3*, edited by R. C. Hwa and X.-N. Wang (World Scientific, Singapore, 2004), p. 634.
- [7] G. Policastro, D. T. Son and A. O. Starinets, Phys. Rev. Lett. **87**, 081601 (2001) [arXiv:hep-th/0104066].
- [8] G. Policastro, D. T. Son and A. O. Starinets, JHEP **0209**, 043 (2002) [arXiv:hep-th/0205052].
- [9] U. Heinz, J. Phys. G **31**, S717 (2005).
- [10] U. W. Heinz and P. F. Kolb, arXiv:hep-ph/0204061.
- [11] C. Eckart, Phys. Rev. **58**, 919 (1940).
- [12] L. D. Landau and E. M. Lifshitz, *Fluid Mechanics*, Sect. 127, Pergamon, Oxford, 1963.
- [13] W. Israel, Ann. Phys. (N.Y.) **100**, 310 (1976); W. Israel and J. M. Stewart, Ann. Phys. (N.Y.) **118**, 349 (1979).
- [14] A. Muronga, Phys. Rev. Lett. **88**, 062302 (2002) [Erratum *ibid.* **89**, 159901 (2002)]; and Phys. Rev. C **69**, 034903 (2004).
- [15] D. A. Teaney, J. Phys. G **30**, S1247 (2004).
- [16] A. Muronga and D. H. Rischke, nucl-th/0407114 (v2).
- [17] U. W. Heinz, H. Song and A. K. Chaudhuri, Phys. Rev. C **73**, 034904 (2006) [arXiv:nucl-th/0510014].
- [18] A. K. Chaudhuri and U. W. Heinz, J. Phys. Conf. Ser. **50**, 251 (2006) [arXiv:nucl-th/0504022].
- [19] A. K. Chaudhuri, Phys. Rev. C **74**, 044904 (2006) [arXiv:nucl-th/0604014].
- [20] A. K. Chaudhuri, arXiv:nucl-th/0703029.
- [21] A. K. Chaudhuri, arXiv:nucl-th/0703027.
- [22] T. Koide, G. S. Denicol, Ph. Mota and T. Kodama, Phys. Rev. C **75**, 034909 (2007).
- [23] R. Baier and P. Romatschke, arXiv:nucl-th/0610108.
- [24] P. Arnold, G. D. Moore and L. G. Yaffe, JHEP **0011**, 001 (2000) [arXiv:hep-ph/0010177].
- [25] G. Baym, H. Monien, C. J. Pethick and D. G. Ravenhall, Phys. Rev. Lett. **64**, 1867 (1990).
- [26] S. R. de Groot, W. A. van Leeuwen and Ch. G. van Weert, *Relativistic Kinetic Theory* (North-Holland, Amsterdam, 1980) p.36